Atmos. Chem. Phys., 13, 12117–12133, 2013
www.atmos-chem-phys.net/13/12117/2013/
doi:10.5194/acp-13-12117-2013

Atmospheric Chemistry and Physics Open Access

A parameterization of sub-grid particle formation in sulfur-rich plumes for global- and regional-scale models

R. G. Stevens[1] **and J. R. Pierce**[1,2]

[1]Department of Physics and Atmospheric Science, Dalhousie University, Halifax, NS, Canada
[2]Department of Atmospheric Science, Colorado State University, Fort Collins, CO, USA

Correspondence to: R. G. Stevens (rgsteven@dal.ca)

Received: 10 July 2013 – Published in Atmos. Chem. Phys. Discuss.: 25 July 2013
Revised: 28 October 2013 – Accepted: 7 November 2013 – Published: 13 December 2013

Abstract. New-particle formation in the plumes of coal-fired power plants and other anthropogenic sulfur sources may be an important source of particles in the atmosphere. It remains unclear, however, how best to reproduce this formation in global and regional aerosol models with grid-box lengths that are tens of kilometres and larger. Based on the results of the System for Atmospheric Modelling (SAM), a large-eddy simulation/cloud-resolving model (LES/CRM) with online two-moment aerosol sectional (TOMAS) microphysics, we have developed a computationally efficient, but physically based, parameterization that predicts the characteristics of aerosol formed within sulfur-rich plumes based on parameters commonly available in global- and regional-scale models. Given large-scale mean meteorological parameters ((1) wind speed, (2) boundary-layer height and (3) downward shortwave radiative flux), (4) emissions of SO_2 and (5) NO_x from the source, (6) mean background condensation sink, (7) background SO_2 and (8) NO_x concentrations, and (9) the desired distance from the source, the parameterization will predict (1) the fraction of the emitted SO_2 that is oxidized to H_2SO_4, (2) the fraction of that H_2SO_4 that forms new particles instead of condensing onto pre-existing particles, (3) the mean mass per particle of the newly formed particles, and (4) the number of newly formed particles per kilogram SO_2 emitted. The parameterization we describe here should allow for more accurate predictions of aerosol size distributions and a greater confidence in the effects of aerosols in climate and health studies.

1 Introduction

It is well known that the size of atmospheric aerosols strongly impacts the magnitude of their direct radiative effect (Charlson et al., 1992) and their ability to act as cloud condensation nuclei (CCN) (Dusek et al., 2006), thereby increasing cloud reflectivity and lifetime (Albrecht, 1989; Twomey, 1974). The uncertainty in the effects of aerosols dominates the uncertainty in radiative forcing changes (Forster et al., 2007). These aerosols are also known to cause respiratory problems in humans (Dockery et al., 1993), and those particles smaller than 100 nm in diameter may have greater health impacts than larger particles (Peters et al., 1997). Thus, it is important to understand aerosol number and size for both climate and health.

One of the largest anthropogenic sources of aerosol mass are sulfur-rich plumes (Dentener et al., 2006). Sulfur dioxide (SO_2) within these plumes can be oxidized by the hydroxyl radical (OH) to form sulfuric acid (H_2SO_4), which in turn can condense onto pre-existing particles. If H_2SO_4 concentrations are high enough, the H_2SO_4 will cluster with itself and other condensible gases to nucleate new particles (Kulmala and Kerminen, 2008). This anthropogenic sulfur has a significant effect on particle concentrations globally, particularly in the Northern Hemisphere (Adams and Seinfeld, 2003; Luo and Yu, 2011; Spracklen et al., 2005; Wang and Penner, 2009).

However, the concentrations of OH are sensitive to NO_x (nitric oxide (NO) + nitrogen dioxide (NO_2)) concentrations, which will vary across a given plume (Lonsdale et al., 2012). Together with the heterogeneity of the condensation sink (approximately proportional to aerosol surface area) within a

plume, this causes the H_2SO_4 concentrations to vary dramatically within a plume. Nucleation and growth rates, which are strong functions of H_2SO_4 concentrations, will in turn vary spatially across a plume. Finally, the coagulation sink of these newly formed particles will also be location-dependant in these plumes, which typically have widths of up to tens of kilometres during the first several hundred kilometres of movement. Currently, global- and regional-scale models typically have resolutions of hundreds and tens of kilometres or more, respectively, and are thus unable to accurately resolve the formation and growth of aerosols within these plumes using grid-box averages for chemical concentrations, aerosol concentrations, and meteorological values.

Therefore, these models have typically assumed that some fraction of all anthropogenic SO_2 emissions are oxidized to form sulfate (SO_4) at the sub-grid scale using a single size distribution for all anthropogenic sulfate sources. For instance, the study of Makkonen et al. (2009) used the assumption recommended by the AeroCom emissions inventory (Dentener et al., 2006): the sulfate was emitted into a single log-normal mode with a median radius of 500 nm and a standard deviation of 2.0. A number of studies (Adams and Seinfeld, 2002, 2003; Pierce and Adams, 2006, 2009; Pierce et al., 2007; Spracklen et al., 2005) have used a bi-modal distribution comprised of a nucleation mode and an accumulation mode with number mean diameters 10 and 70 nm, and geometric standard deviations 1.6 and 2.0. Either 5 or 15 % of the sulfate mass is emitted into the nucleation mode, depending on the study. Yet another approach was used in the study of Yu and Luo (2009): they emitted 5 % of sulfur mass into the aforementioned nucleation mode and condensed the remaining mass onto the existing accumulation-mode particles. As some of the sulfate formed in the plume must condense onto the pre-existing particles that have been entrained into the plume, this approach is, in this way, more realistic than the other assumptions.

While the studies listed above differ in the amount and size of sub-grid sulfate particles, they all assume that these values are constant regardless of the meteorological and chemical characteristics of the emissions plumes. However, several studies have shown that the particle formation in plumes is strongly sensitive to environmental conditions. Yu (2010) showed that differences in temperature and hydroxyl concentrations cause the size and number of aerosol particles to vary seasonally and diurnally. Lonsdale et al. (2012) showed that the number of particles formed within sulfur-rich plumes is strongly dependent on the emission rates of both SO_2 and NO_x from the source. In addition, we have shown in Stevens et al. (2012) that the background aerosol concentrations and the meteorology have strong effects on number and size of aerosol formed within such plumes. However, there is currently no means of representing these dependencies of plume-scale particle formation in global and regional models.

Several global studies have already investigated the sensitivity of global CCN concentrations to the assumptions made regarding sub-grid sulfate formation. Luo and Yu (2011) varied the fraction of emitted sulfate that was emitted into the nucleation mode from 5 to 15 % and found that this increased the CCN at an assumed supersaturation of 0.2 % (CCN(0.2 %)) by up to 18 % over source regions. Furthermore, they found that changing the fraction of emitted SO_2 converted to sub-grid sulfate from 0 to 5 % changed global boundary-layer CCN(0.2 %) by 11 %. The earlier studies of Adams and Seinfeld (2003) and Spracklen et al. (2005) used the 10 and 70 nm mode sub-grid sulfate assumptions described above. Each found that if the fraction of SO_2 converted to sub-grid sulfate was changed from 0 to 3 %, CCN(0.2 %) in polluted areas would double. Adams and Seinfeld (2003) included only sulfate aerosol in their model, and Spracklen et al. (2005) included only sulfate and sea-salt aerosol, so this was believed to be an upper limit for this effect. However, the study of Wang and Penner (2009), which included organic matter, black carbon, and dust, varied the fraction of SO_2 converted to sub-grid sulfate over a smaller range (0 to 2 %), and also found that CCN(0.2 %) more than doubled over polluted areas. Additionally, they found that CCN(0.2 %) increased by 23 to 53 % averaged over global boundary layer and that the aerosol indirect effect radiative forcing increased by 11 to 31 % (depending on the grid-resolved nucleation scheme used in the boundary layer). CCN concentrations and regional radiative forcings are thus clearly sensitive to the assumptions regarding sulfur partitioning and the size of aerosol formed in sulfur-rich plumes.

Lee et al. (2013) recently quantified the uncertainty in CCN concentrations that was due to 28 different uncertain inputs in the GLOMAP global aerosol model. Based on the results of Stevens et al. (2012), the range of possible values for the diameter of sub-grid sulfate particles used in Lee et al. (2013) was reduced to a smaller range than the full range of sub-grid-sulfate assumptions used previously in studies, which lead to a reduced estimation of the uncertainty in CCN concentrations attributable to this input compared to the range of estimates described in the previous paragraph. Even with the reduced ranges, the uncertainties in sub-grid SO_4 production were found to be just as important as the uncertainties in SO_2 emission rates and had the largest contribution of the 28 inputs to the uncertainty in CCN concentrations over polluted North America and Europe. Globally, the uncertainty in sub-grid-sulfate particle size ranked as the twelfth-largest contributor to the relative uncertainties in CCN concentrations of the 28 inputs tested, with a global-mean relative uncertainty range (from -2 to $+2$ standard deviations in CCN concentrations) of about 16 %. These large uncertainties in CCN prediction due to sub-grid sulfate formation highlight the need for improved representation of plume-scale particle formation in global and regional models.

In this paper, we develop a computationally efficient (the increase in running time for a 3-D aerosol model would be negligible because the parameterization consists only of several arithmetic equations), but physically based, parameterization that predicts the characteristics of aerosol formed within sulfur-rich plumes based on parameters commonly available in global- and regional-scale models. This parameterization is based on the results of the System for Atmospheric Modelling (SAM) (Khairoutdinov and Randall, 2003), a large-eddy simulation/cloud-resolving model (LES/CRM) with online two-moment aerosol sectional (TOMAS) microphysics (Adams and Seinfeld, 2002) that has been tested against aircraft observations of particle formation in plumes (Lonsdale et al., 2012; Stevens et al., 2012). Given large-scale mean meteorological parameters ((1) wind speed, v_g [$\mathrm{m\,s^{-1}}$], (2) boundary-layer height, BLH [m], and (3) downward shortwave radiative flux, DSWRF [$\mathrm{W\,m^{-2}}$]), (4) emissions of SO_2, SO_2 emis [$\mathrm{kg\,s^{-1}}$], and (5) NO_x, NO_x emis [$\mathrm{kg\,N\,s^{-1}}$], from the source; (6) mean background condensation sink, CS [$\mathrm{s^{-1}}$]; (7) mean background SO_2, bgSO_2 [ppb], and (8) NO_x, bgNO_x [ppb], concentrations; and (9) the desired distance from the source, d [m]; the predicting particle production in power-plant plumes (P6) parameterization predicts (1) the fraction of the emitted SO_2 that is oxidized to form H_2SO_4, f_{ox}; (2) the fraction of that H_2SO_4 that forms new particles instead of condensing onto pre-existing particles, f_{new}; (3) the mean mass per particle of the newly formed particles, M_m [kg]; and (4) the number of newly formed particles per mass of SO_2 emitted, N_{new} [$\#\,\mathrm{kg^{-1}}$ SO_2].

In Sect. 2 we provide a brief description of the SAM-TOMAS model and how the P6 training data were selected. Section 3 describes the form and physical basis of the P6 parameterization. The evaluation of the P6 parameterization against the full SAM-TOMAS model is presented in Sect. 4. We describe sensitivity studies performed using the parameterization in Sect. 5. Finally, we present our conclusions in Sect. 6.

2 Description of SAM-TOMAS model and training data

A full description of the SAM-TOMAS model is available in Stevens et al. (2012), so we will restrict ourselves to a brief summary here. The SAM model (Khairoutdinov and Randall, 2003) is a flexible LES/CRM model with a resolution of tens of metres to several kilometres and a domain that can span tens to hundreds of kilometres. The TOMAS microphysics algorithm (Adams and Seinfeld, 2002; Pierce and Adams, 2009) in SAM resolves aerosol by both mass and number independently in 15 size bins spanning 3 to 10 µm. Condensation, coagulation, and nucleation are explicitly resolved in the model. Sulfate, ammonium (NH_3), aerosol water, and the gas-phase concentrations of SO_2, NO_x, ammonia (NH_4), and H_2SO_4 are simulated within the model, but secondary organic aerosol formation is not explicitly simulated under the assumption that sulfate aerosol formation will dominate within sulfur-rich plumes.

The concentration of OH in the SAM-TOMAS model is currently parameterized based on the downward shortwave radiative flux (DSWRF) and the concentration of NO_x. This OH parameterization is an empirical fit to results from the detailed time-dependent photochemical box model described by Olson et al. (2006). However, the uncertainties associated with the parameterized OH become large for solar zenith angles larger than 70°, which, for clear-sky conditions, correspond to DSWRF values less than $350\,\mathrm{W\,m^{-2}}$. In addition, we do not account for nitrous acid (HONO) or sulfur trioxide (SO_3) emission, which may account for additional sulfuric acid formation. Both of these emissions may result in particle formation early in the plume, and may account for the under-prediction of particles within 5 km of the stack in Stevens et al. (2012). However, we note that these processes do not seem to be necessary to accurately predict particle size and number concentrations beyond 30 km from the source. When these processes become better understood, we plan to incorporate them into a future version of the P6 parameterization.

During cloudy conditions, SO_2 may undergo aqueous oxidation through reaction with H_2O_2 or other species (Zhou et al., 2012). Currently, this is not accounted for in the SAM-TOMAS model. Therefore, SO_2 oxidation is likely underestimated under cloudy conditions. Under such conditions, however, less new-particle formation is expected because DSWRF and subsequently oxidation of SO_2 though reaction with OH will also be suppressed. Also, the additional surface area from cloud droplets in the clouds and cloud-processed aerosols outside of the clouds will slow nucleation and increase coagulational losses of new particles. We therefore do not believe that this would be a significant uncertainty for predicting the number and size of aerosol formed in sulfur-rich plumes.

For this study, the model was operated as a Lagrangian 2-D wall model that passed over the power plant after a spin-up period of 1800 s of model time. The wall extends upwards and horizontally perpendicular to the direction of the mean boundary-layer wind. We have evaluated the model operating in Lagrangian mode against the Eulerian mode used in Stevens et al. (2012), and we have found that the discrepancies in NO_x and SO_2 concentrations between the two models are less than one standard deviation of the concentrations (due to variability in time). Similarly, the total particle concentration within the plume differed by less than 16 % between the Lagrangian and the Eulerian modes, and the particle size distributions had similar characteristics in both models. Both models compare similarly well to the measurements shown in Stevens et al. (2012).

In the simulations used here, the model resolution was held fixed at $400\,\mathrm{m} \times 400\,\mathrm{m} \times 40\,\mathrm{m}$ and the model domain was 120 km wide and 5 km high. We chose an empirical

activation-type nucleation scheme (Kulmala et al., 2006), where nucleation rates are calculated as $10^{-7}\,s^{-1}\cdot[H_2SO_4]$ because this scheme provided the best match to observations out of the six schemes tested in Stevens et al. (2012). We note that it is clear that such an empirical scheme will not capture all of the variability in nucleation rates. However, an increase in the nucleation rate by a factor of 10 was found in Stevens et al. (2012) to increase N_{new} by a factor of about 3 for distances greater than 30 km from the source, and we will show that values of N_{new} span six orders of magnitude across the set of training data used for this study. As more accurate parameterizations of nucleation become available, we plan to integrate them into SAM-TOMAS and incorporate the results into future versions of the P6 parameterization.

In order to determine the best-fit parameters for the P6 parameterization, we performed many simulations using the SAM-TOMAS model using a realistic range of different inputs for the emissions, meteorology, and background aerosol and trace gas concentrations. In order to choose realistic, but sufficiently diverse, conditions for the simulations, we performed the procedure described in the following three paragraphs.

To generate a data set of realistic aerosol size distributions and trace gas concentrations, we used output from the GEOS-Chem-TOMAS model. GEOS-Chem-TOMAS uses the TOMAS aerosol microphysics module described above in the GEOS-Chem chemical transport model (www.geos-chem.org; Bey et al., 2001). The implementation of TOMAS in GEOS-Chem has been discussed previously (Pierce et al., 2013; Snow-Kropla et al., 2011; Trivitayanurak et al., 2008). Variables were output every 3 h. The model resolution was $0.5^\circ \times 0.666^\circ$. We used Latin hypercube sampling (a method of pseudo-randomly choosing a set of samples from a multi dimensional space such that the full range of each dimension is sampled, but the coordinates in each dimension are uncorrelated) to determine a set of 5000 (1) latitudes, (2) longitudes, (3) dates and times, (4) distances from the emissions source (d), (5) emissions rates of SO_2 (SO_2 emis) and (6) NO_x (NO_x emis), and (7) effective emissions heights, which implicitly includes both the height of the emissions stack and the initial buoyant rise of the plume. The range of values used for each of these variables is listed in Table 1. We note that while only the month of July was sampled to create the training data, the large geographic range used provided diverse meteorological conditions. As the OH parameterization used in the SAM-TOMAS model has high uncertainties for large solar zenith angles, we excluded the hours of 03:00, 06:00, and 09:00 UTC from our range of times to be selected as these should be at high solar zenith angles or outside daylight hours for the latitude and longitude range we selected. In order to further reduce the number of cases with high solar zenith angles, we subsequently excluded from our analysis any cases that had DSWRF values less than $100\,W\,m^{-2}$. We then obtained the background aerosol size distribution, background SO_2 and NO_x concentrations ($bgSO_2$ and $bgNO_x$), and DSWRF from the GEOS-Chem-TOMAS output that corresponded to each set of latitude, longitude, date, and time. The maximum, minimum, and median values of these outputs from GEOS-Chem-TOMAS are shown in Table 2.

Table 1. Parameter space used to create training data for the P6 parameterization.

Parameter	Minimum	Maximum
Latitude	30° N	70° N
Longitude	55° W	110° W
Time	1 July 2010, 15:00 UTC	28 July 2010, 21:00 UTC
Distance from source	5 km	100 km
$\log_{10}(SO_2$emis $[kg\,s^{-1}])$	−3	1
$\log_{10}(NO_x$emis $[kg\,N\,s^{-1}])$	−3	0.3
Emissions height	60 m	580 m

To drive the dynamics in SAM-TOMAS, we obtained for each set of latitude, longitude, date, and time (1) the corresponding profiles of potential temperature, water vapour mixing ratio, wind speed and direction; (2) the surface fluxes of sensible heat, latent heat, and momentum; and (3) the boundary-layer height (BLH) and the surface pressure from the National Center for Environmental Prediction (NCEP) North American Regional Reanalysis (NARR) (Mesinger et al., 2006) assimilated meteorology data, as was done for the study of Stevens et al. (2012). The reanalysis data were provided by the National Oceanic and Atmospheric Administration (NOAA), Ocean and Atmospheric Research (OAR), Earth System Research Laboratory (ESRL) Physical Sciences Division (PSD) (Boulder, Colorado, USA) from their website at: http://www.esrl.noaa.gov/psd/. The NCEP NARR data were chosen for this study because the software necessary to create input files from reanalysis data was readily available. We note that while the meteorology from the reanalysis data may not correspond exactly to the data from the GEOS-Chem-TOMAS model due to differences in spatial and temporal resolution, an exact match is not necessary to create a realistic set of training inputs.

For each simulation using the SAM-TOMAS model, we used SO_2emis, NO_xemis, and effective emissions height from the Latin hypercube sample; the background aerosol size distribution, $bgSO_2$, $bgNO_x$, and DSWRF from the output of the GEOS-Chem-TOMAS model; and the SAM-TOMAS meteorology that was driven by nudging and boundary conditions from the NCEP-NARR assimilated meteorology data. We ran the model until the emissions reached the distance from the source specified from the Latin hypercube sample. We preserved the following variables as training inputs for the P6 parameterization: (1) SO_2emis, (2) NO_xemis, (3) total condensation sink of the background aerosol size distribution (CS), (4) DSWRF, (5) the mean wind speed

Table 2. Outputs from GEOS-Chem-TOMAS used as inputs for SAM-TOMAS. The fully resolved aerosol size distribution from GEOS-Chem-TOMAS was used in SAM-TOMAS, but for conciseness we only tabulate the condensation sink here. Cases where the DSWRF was less than 100 were excluded from this study because of uncertainties associated with OH production for these conditions.

Parameter	Minimum	Maximum	Median
Condensation sink [s^{-1}]	8.94×10^{-5}	1.46×10^{-2}	1.38×10^{-3}
Background SO_2 [ppb]	1.27×10^{-6}	16.6	0.0707
Background NO_x [ppb]	2.84×10^{-4}	7.93	0.0302
DSWRF [$W\,m^{-2}$]	100	960	401

Table 3. Minimum, maximum, and median values of the mean boundary-layer wind speeds and the boundary-layer heights for the training data used in this study.

Parameter	Minimum	Maximum	Median
Wind speed [$m\,s^{-1}$]	0.178	26.1	5.98
Boundary-layer height [m]	53	2792	434

within the boundary layer (v_g), (6) BLH, (7) the distance from the source (d), (8) bgSO_2, and (9) bgNO_x. The maximum and minimum values of these parameters are shown in Tables 1, 2, and 3. Other information necessary to run the SAM-TOMAS model – such as the effective emissions height, the potential temperature profile, the water vapour mixing ratio profile, and the surface fluxes – may not be available in many regional- and global-scale models and the current P6 inputs capture most of the variability in aerosol formation and growth within plumes, as we will show in Sect. 5. We have therefore excluded them as inputs to the parameterization. However, by including a wide range of these conditions in the simulations used to fit the parameterization, we hope to exclude a possible bias in our predictions, and to have a more realistic assessment of the accuracy of the parameterization.

3 Description of the parameterization

The purpose of the P6 parameterization is to predict the fraction of emitted SO_2 that is oxidized in the plume (f_{ox}), whether or not a significant number of new particles are nucleated, the number of new particles nucleated per kg SO_2 emitted (N_{new}, [#/kg SO_2]), the mean mass per particle of the new particles (M_m, [kg]), and the fraction of the H_2SO_4 formed within the plume that comprises new particles (f_{new}).

As inputs to the parameterization, we have chosen variables that are commonly available in global- and regional-scale models: the source-level SO_2 and NO_x emissions (SO_2emis [$kg\,s^{-1}$] and NO_xemis [$kg\,N\,s^{-1}$]), the downward shortwave radiative flux at the surface (DSWRF [$W\,m^{-2}$]), the background aerosol condensation sink (CS [s^{-1}]), the boundary-layer height (BLH [m]), the mean wind speed in the boundary layer (v_g [$m\,s^{-1}$]), the distance from the source (d [m]) at which the plume is considered mixed with the model grid boxes, and the background SO_2 and NO_x concentrations (bgSO_2 [ppb] and bgNO_x [ppb]). We will consistently use the given units for all inputs and outputs in all of the following equations.

Table 4. Emissions rates for coal-fired power plants in the USA from the 2010 EPA CAM data. "Medium" emissions are defined as the log-space mean, "high" as one standard deviation above the mean, and "low" as one standard deviation below the mean.

	SO_2	NO_x
high	$1.00\,kg\,s^{-1}$	$0.290\,kg\,s^{-1}$
medium	$0.202\,kg\,s^{-1}$	$0.0840\,kg\,s^{-1}$
low	$0.0606\,kg\,s^{-1}$	$0.0300\,kg\,s^{-1}$

Often, emissions inventories provide SO_2 and NO_x emissions within each box on a given grid, instead of associated with particular sources specifically. Therefore, it may not be known how many power plants are responsible for the emissions in a given grid box. We therefore allow the P6 parameterization to be operated in the following ways: (1) by default, it is assumed that the emissions of each anthropogenic sulfur-rich point source are known individually, in which case f_{ox}, N_{new}, M_m, and f_{new} will be predicted for each source plume individually. (2) If instead the total emissions of SO_2 and NO_x from sulfur-rich sources within a given area (but not the individual sources within that area) are known, the P6 parameterization will provide outputs based on the assumption that the emissions for the sources are divided between an equal number of high, medium, and low emitters. We define high, medium, and low emitters based on the emissions data for power plants in the United States compiled from the Clean Air Markets (CAM) data (United States Environmental Protection Agency, 2012) as follows: for medium emitters, we use the log-space mean emission rates for a power plant in the USA during 2010. For low and high emitters, we use an emission rate that is one standard deviation below or above the mean in log space, respectively. The high, medium, and low emission rates are listed in Table 4. (3) If the SO_2 emissions are known, but the NO_x emissions are not known (or the NO_x emissions from the major SO_2 sources are not known), the median $SO_2 : NO_x$ emissions ratio of 0.419 from the 2010 EPA CAM data will be assumed (as well as the high-, medium-, and low-emitter assumptions from the previous P6 mode).

Even if the precise locations of power plants are known, it may not be clear at what distance from the source the particles are well mixed within a grid box that also contains the source of emissions. However, as we will show in Sect. 5, the P6 values of M_m, N_{new}, and f_{new} are not strongly sensitive to the distance from the source beyond distances of 30 km,

Table 5. Emission scaling factors used in the P6 parameterization for determining effective SO_2 and NO_x concentrations (Eqs. 1 and 9).

	NO_xemis scaling factor	SO_2emis scaling factor
In-plume mean concentration	9.595×10^4	1.705×10^4
f_{ox}	1.444×10^{-8}	–
nucleation	4.365×10^5	2.239×10^4
M_m	2.139×10^7	2.605×10^6
N_{new}	1.243×10^6	–

and f_{ox} depends less than linearly on the distance from the source.

In the following subsections, we describe the theory and semi-empirical fits behind the P6 parameterization.

3.1 Fraction oxidized

In order to formulate a semi-empirical equation for f_{ox}, we first formulate a semi-empirical equation for the effective NO_x mixing ratio within the plume because NO_x modulates the OH concentrations and thus affects the oxidation rate of SO_2. The mean concentration of NO_x within the plume should be equal to the sum of the contributions from the background and the emitted NO_x after accounting for dilution, which should be related to v_g, BLH, and the time since emission, calculated as (d/v_g). We therefore calculate the effective NO_x concentration, $NO_{x,eff}$ [ppb], as

$$NO_{xeff} = bgNO_x + 1.444 \times 10^{-8} \frac{NO_x emis}{v_g^{1.234} BLH^{0.2018} \left(\frac{d}{v_g}\right)^{0.7902}}, \quad (1)$$

where the exponents for v_g, BLH, and (d/v_g) have been fitted for this equation to the average concentrations of NO_x in the plume using the training data (evaluation of the fit in Sect. 4). We allowed the scaling factor of 1.444×10^{-8} to be freely fitted to the data because the relative importance of the background concentrations and the emitted NO_x is different for the f_{ox} than it is for the mean concentration of NO_x. As the relative importance of background and emitted NO_x is also different for determining nucleation, M_m, and N_{new}, we list the scaling factors used to calculate $NO_{x,eff}$ for each of these outputs in Table 5. The scaling factor found when fitting to the mean NO_x concentration within the plume was 9.595×10^4. However, the best-fit scaling factor found for calculating f_{ox} is much lower, such that the $NO_{x,eff}$ is dominated by $bgNO_x$. Generally, NO_x concentrations are sufficiently high within the centre of the plume (and early in the plume) to prevent fast oxidation of SO_2, so the background concentrations are relatively much more important to f_{ox} than they are to the mean NO_x concentration within the plume.

We calculate an effective OH concentration using the same parameterization that is used in the SAM-TOMAS model. This parameterization calculates the OH concentration as a function of the NO_x concentration within the plume and the DSWRF. The parameterization, which is a fit of chemistry box-model simulations of Olson et al. (2006), was originally described in Appendix A of Stevens et al. (2012).

First, we set variables x and y:

$$x = \log\left(NO_{x,eff}\right) - 0.195, \quad (2)$$

$$y = \frac{DSWRF}{S_0 \cdot T}, \quad (3)$$

where S_0 is the solar constant at the top of the atmosphere, $1370\,W\,m^{-2}$, and T is an assumed transmittance of the clear atmosphere, 0.76. We then calculate two polynomials, the first (P1) estimating the shape of the OH versus NO_x relationship, and the second (P2) capturing the dependance of OH on DSWRF:

$$P1 = -0.014x^6 + 0.0027x^5 + 0.1713x^4 - 0.0466x^3 \quad (4)$$
$$- 0.7893x^2 - 0.1739x + 6.9414,$$

$$P2 = \left(-1345y^3 + 4002y^2 - 471.8y + 42.72\right) \times 10^4. \quad (5)$$

From P1 and P2, we calculate the effective OH concentration, OH_{eff}, [molec cm^{-3}]:

$$OH_{eff} = 0.82 \cdot 10^{P1 \cdot \log(P2)/6.8}. \quad (6)$$

If we assume that the only loss mechanism for SO_2 is through reaction with OH (e.g. clear skies and ignore reactions with Criegee intermediates; Mauldin et al., 2012), and we knew the true OH concentrations, we could calculate f_{ox} by using the rate constant k, the time elapsed t, and the following equation:

$$f_{ox} = 1 - \exp\left(-k\,[OH]\,t\right). \quad (7)$$

However, given that OH_{eff} is not the true concentration, and that we must calculate t as d/v_g, we use the analogous equation

$$f_{ox} = 1 - \exp\left(-1.650 \times 10^{-10} OH_{eff}^{0.7904} \left(\frac{d}{v_g}\right)^{0.7723}\right), \quad (8)$$

where the numerical values have been selected by minimizing the error between the P6 fit f_{ox} values and the predicted f_{ox} from the SAM-TOMAS simulations. As the best-fit NO_xemis scaling factor for calculation of $NO_{x,eff}$ is near zero, OH_{eff} is approximately equal to the OH concentration outside of the plume in the f_{ox} calculation. NO_x concentrations will generally be high enough within the plume for OH concentrations within the plume to be less than the OH concentrations at the plume edges, and therefore the best fit exponent for OH_{eff} is less than one. Oxidation of SO_2 subsequently proceeds more slowly within the plume than at the edges, and thus the best-fit exponent for (d/v_g) is also less than 1.

3.2 Nucleation

In order to determine whether or not significant nucleation occurs within the plume, we first calculate the effective NO_x and SO_2 concentrations within the plume. The effective SO_2 concentration, $SO_{2,\mathrm{eff}}$ [ppb], is defined similarly to $NO_{x,\mathrm{eff}}$ as

$$\mathrm{SO_{2\,eff}} = \mathrm{bgSO_2} + 2.239 \times 10^4 \frac{\mathrm{SO_2\ emis}}{v_g^{1.229}\mathrm{BLH}^{0.1891}\left(\frac{d}{v_g}\right)^{0.7732}}, \quad (9)$$

where the exponents for v_g, BLH, and (d/v_g) have been fitted for this equation to the average concentration of SO_2 in the plume. The scaling factor found when fitting to the mean SO_2 concentration within the plume was 1.705×10^4. The scaling factors for $SO_{2\mathrm{eff}}$ and $NO_{x,\mathrm{eff}}$ for determining nucleation are 2.239×10^4 and 4.365×10^5, respectively, as listed in Table 5.

We then calculate nucp, our predictor for whether nucleation is likely, from the following equation:

$$\mathrm{nucp} = \frac{\left(\mathrm{SO_{2,eff}}\right)^{1.92}\mathrm{dswrf}^{3.28}}{\left(\mathrm{NO_{x,eff}}\right)^{1.24}\mathrm{CS}^{3.48}}. \quad (10)$$

We compare the value of nucp to 2.988×10^{14}. If it is smaller, then we predict that nucleation is slow and that any particles that are formed within the plume will be quickly lost to coagulation: there will be no net increase in particle number within the plume. If it is larger, we predict that significant new-particle formation will occur. This test is accurate for 95.8 % of our training cases. For those cases where nucleation is falsely predicted or falsely not predicted, the maximum P6 or SAM-TOMAS values of M_m, respectively, were less than the median values of M_m for the full set of training data. The maximum number of new particles formed was similarly lower than the median for the full set of training data. Particle formation rates and growth rates were therefore typically lower for the cases where this test was incorrect than for the correctly predicted cases.

3.3 Mean mass per particle of new particles

If we predict that there will be significant nucleation, we then predict the mean mass per particle of the newly formed particles. We expect that the particles will be growing primarily through condensation of available H_2SO_4. Therefore, we expect that the mean mass per particle, M_m, will be proportional to the product of the time elapsed (d/v_g), f_ox, and $SO_{2\mathrm{eff}}$. Since the pre-existing particles will be competing for the available H_2SO_4, we divide this value by the background condensation sink, CS, the first-order rate constant of the loss of condensible vapour by condensation, which is proportional to the Fuchs-corrected surface area of the particles (Kerminen et al., 2004). We add a constant minimum value to this, which corresponds to the smallest size of aerosol that can be resolved by the SAM-TOMAS model. In this way we arrive at the following equation for M_m:

$$M_\mathrm{m} = 1.475 \times 10^{-27}\frac{f_\mathrm{ox}^{1.517}\mathrm{SO}_{2,\mathrm{eff}}^{1.094}}{\mathrm{CS}^{0.6173}}\left(\frac{d}{v_g}\right)^{0.9685} + 4.071 \times 10^{-23}\mathrm{kg}. \quad (11)$$

Again, we include the fitted parameters in this equation, and the fit will be evaluated in Sect. 4.

However, we note that the free parameters for predicting f_ox were optimized to reduce the root-mean-square (rms) absolute error between the parameterized f_ox and the SAM-TOMAS predicted f_ox to a minimum, and we are more interested in minimizing the rms relative error in M_m, since M_m spans several orders of magnitude. We therefore allowed the free parameters used to predict f_ox to change when we sought the parameters that minimize the rms error in $\log_{10}(M_\mathrm{m})$. Notably, the NO_xemis scaling factor (Eq. (1)) used within the calculation of M_m is several orders of magnitude larger than that used within the calculation of f_ox, as listed in Table 5. We will discuss this difference further in Sect. 5.

We can calculate the mass mean diameter D_mass [µm] as

$$D_\mathrm{mass} = \left(\frac{M_\mathrm{m}}{\rho}\frac{6}{\pi}\right)^{\frac{1}{3}}, \quad (12)$$

where ρ is the density of the dry aerosol (assumed in SAM-TOMAS as 1770 kg m^{-3}). The number-median diameter D_m [µm] can be calculated from

$$D_\mathrm{m} = D_\mathrm{mass}\exp\left(-1.5\ln^2\sigma_g\right), \quad (13)$$

where σ_g is the geometric standard deviation of the aerosol size distribution. We choose a value of 1.4 for σ_g, as this was the median value found for log-normal distributions fitted to the aerosol size distributions of the training data.

3.4 Number of new particles per kg SO_2 emitted

As mentioned in Sect. 2, we have configured the SAM-TOMAS model to use activation-type nucleation for this study. We would therefore expect the source of new particles to increase due to nucleation proportionally with the concentration of H_2SO_4, which should be roughly proportional to f_ox. We would therefore expect a solution that is proportional to f_ox and increases with increasing $\mathrm{bgSO_2}$, but not SO_2emis, as N_new is normalized by the SO_2 emissions. We also expect the primary loss mechanism for the newly formed particles to be coagulation with pre-existing particles, and this coagulational loss rate is roughly proportional to the condensation sink. We would therefore also expect the solution to exponentially decay with CS (d/v_g). We find the following solution for N_new:

$$N_\mathrm{new} = 6.939 \times 10^{23} \quad (14)$$
$$\frac{f_\mathrm{ox}^{0.9949}\mathrm{bgSO}_2^{0.2500}}{\mathrm{SO_2emis}^{0.1280}}\exp\left(-4.417\mathrm{CS}^{0.1441}\left(\frac{d}{v_g}\right)^{0.1736}\right),$$

Table 6. Quality of fit information for the P6 parameterization predicted outputs and the results of SAM-TOMAS.

	correlation coefficient	rms error	rms $\log_{10}$ error	fraction within a factor of 2	fraction within a factor of 10
f_{ox}	0.826	0.0190	0.845	50.3 %	77.0 %
M_m	0.891	1.38×10^{-19} kg	0.425	60.0 %	96.7 %
N_{new}	0.670	4.85×10^{18} $(kg\,SO_2)^{-1}$	0.741	36.2 %	84.6 %
f_{new}	0.650	0.289	1.07	28.6 %	66.8 %

where the free parameters for f_{ox} have been fitted to minimize the rms error in $\log_{10}(N_{new})$, as was the case for M_m above. Similar to M_m, the NO_xemis scaling factor (Eq. (1)) used to calculate f_{ox}in N_{new} is several orders of magnitude greater than that used to calculate f_{ox}, as listed in Table 5. This will be discussed further in Sect. 5. We note that the P6 fit value for N_{new} slightly decreases with increasing SO_2emis. As N_{new} is normalized by the SO_2 emissions, this is consistent with the number of new particles formed in a given plume increasing slightly less than linearly with increasing SO_2 emissions.

3.5 Fraction of sulfate mass that comprises new particles

The mass of new particles per kg SO_2 emitted can be determined from the product of M_m and N_{new}. The product of f_{ox} and f_{new} also yields the mass of SO_2 that ultimately forms new particles per kg SO_2 emitted. We therefore can calculate f_{new} from the other three outputs:

$$f_{new} = \frac{M_m N_{new}}{f_{ox}} \frac{M_{SO_2}}{M_{H_2SO_4}},$$

where M_{SO} and $M_{H_2SO_4}$ are the molar masses of SO_2, and H_2SO_4, respectively.

However, because the fits for M_m, N_{new} and f_{ox} were performed independently, this equation can yield values for f_{new} greater than 1 under some conditions, which is unphysical. Under such circumstances, we reduce M_m and N_{new} each by a factor of $f_{new}^{0.5}$ to maintain closure, and limit f_{new} to 1.

4 Comparison of parameterization to full SAM-TOMAS model

We show the correlation coefficient, rms error, rms error in the logarithm of the values, and the fraction of the training data cases within a factor of 2 or 10 for each of the outputs in Table 6. We also show the P6 predicted values against the SAM-TOMAS calculated values for f_{ox}, M_m, N_{new}, and f_{new} in Fig. 1. We show the values of M_m, N_{new}, and f_{new} only for cases where nucleation is predicted to occur.

The correlation between the P6 and SAM-TOMAS values of f_{ox} is good ($R = 0.826$). The rms error is comparable to the value of f_{ox} for the majority of the training cases, but this value is dominated by the small number of cases where either the P6 value, the SAM-TOMAS value, or both values of f_{ox} are large. As can be seen in Fig. 1a, a large fraction (69 %) of cases have both P6 and SAM-TOMAS f_{ox} less than 0.02, and the relative error can be large for these cases, while the absolute error remains low.

The correlation between the P6 and SAM-TOMAS values of M_m is also good ($R = 0.864$). While the SAM-TOMAS values of M_m span more than five orders of magnitude, we note that the P6 values are within one order of magnitude of the SAM-TOMAS values for nearly all (96.8 %) of the training cases, and for the majority of the cases (59.5 %), they are within a factor of two. Along with the P6 and SAM-TOMAS values of M_m, we also plot the values used by Dentener et al. (2006) and Adams and Seinfeld (2003) for M_m in Fig. 1b. We note that the value of M_m from Dentener et al. (2006) is more than three orders of magnitude larger than the largest value calculated by SAM-TOMAS for the training simulations. The value from Adams and Seinfeld (2003) is within the range of values predicted by SAM-TOMAS, but is more than two orders of magnitude larger than the median value of M_m for the training simulations. There is a large fraction of new-particle-formation cases (40 %) where both P6 and SAM-TOMAS values of M_m do not exceed 2×10^{-22} kg, corresponding to a mass mean diameter of less than 6 nm.

While the P6 parameterization does not capture the behaviour of N_{new} as well as it captures the behaviour of f_{ox} and M_m, the P6 values are still within one order of magnitude of the SAM-TOMAS values for most (83.8 %) of the training cases, across which the SAM-TOMAS values vary by more than six orders of magnitude. In addition to the P6 and SAM-TOMAS values of N_{new}, we also plot the values used by Dentener et al. (2006) and Adams and Seinfeld (2003) for N_{new} in Fig. 1c. We note that the value of N_{new} from Dentener et al. (2006) is more than two orders of magnitude smaller than the smallest value calculated by SAM-TOMAS for the training simulations. The value from Adams and Seinfeld (2003) is within the range of values predicted by SAM-TOMAS, but is nearly one order of magnitude larger than the median value of N_{new} for the training simulations.

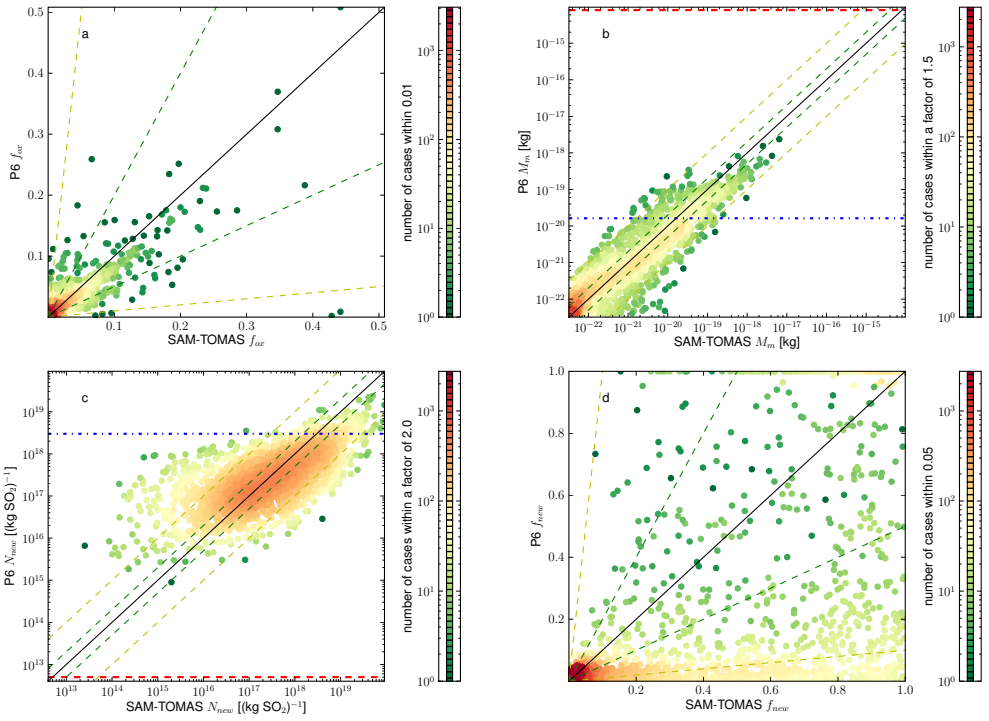

Fig. 1. P6 vs SAM-TOMAS values of f_{ox}, M_{m}, N_{new}, and f_{new}. Colour of points indicates density of cases. The red dashed lines indicate the values of M_{m} and N_{new} from Dentener et al. (2006), and the blue dash-dotted lines indicate the values of M_{m} and N_{new} from Adams and Seinfeld (2003). The green and yellow dashed lines indicate where the predicted values are within a factor of 2 and 10, respectively, of the calculated values.

As the P6 values of f_{new} are calculated based on f_{ox}, M_{m}, and N_{new}, instead of being fitted directly to the SAM-TOMAS values, we would expect this variable to show the poorest fit to the SAM-TOMAS values. Since f_{ox} and f_{new} are uncorrelated, there will be instances where the value of f_{ox} is small, and hence the relative error in f_{ox} may be high, but the value of f_{new} is not small. Since f_{new} is calculated using f_{ox}, a large relative error in f_{ox} will yield a high relative error in f_{new}, and so this means that the relative error in f_{new} can be high, even for larger values of f_{new} (hence the absolute error will also be large). However, the correlation between the P6 and SAM-TOMAS f_{new} values remains good ($R = 0.667$) largely due to resolving the cluster of values near 0 and the cluster near 1 (Fig. 1d). The P6 parameterization correctly predicts low values for f_{new} for the large fraction (56 %) of training cases where the SAM-TOMAS value of f_{new} is less than 0.1, and the P6 value of f_{new} is within 0.1 of the SAM-TOMAS value for 63.3 % of the cases.

5 Sensitivity studies

5.1 Sensitivities to inputs

We show the sensitivities of f_{ox}, M_{m}, N_{new}, and f_{new} to each of the P6 inputs in Figs. 2, 3, 4, and 5, respectively. Each figure shows green lines for 100 randomly chosen sets of inputs within the ranges of the training data. The black line shows the sensitivity from the set of median values for each input (SO_2emis = 0.1 kg s^{-1}, NO_xemis = 0.05 kg s^{-1}, d = 50 km, other values shown in Tables 2 and 3). In each panel, one of the input variables is varied while the others are held fixed. In order to highlight the sensitivities to the inputs, each plotted line is shifted vertically to the centre of the subplot. For Fig. 2 (f_{ox}) and Fig. 5 (f_{new}), we subtract the median value of each line from its values. For Fig. 3 (M_{m}) and Fig. 4 (N_{new}), each plotted line is divided by its median value. We do not show values for M_{m}, N_{new}, or f_{new} where nucleation is not predicted to occur by the P6 parameterization. Therefore, some lines begin or end in Figs. 3, 4, and 5 as the threshold for nucleation is crossed (Eq. 10)

The value of f_{ox} (Fig. 2) is insensitive to SO_2emis, CS, and bgSO_2, as one would expect. The value of f_{ox} is also insensitive to NO_xemis. As we note in Sect. 3.1, oxidation generally proceeds much more quickly at the plume edges and in the dilute plume than at the plume centre, so f_{ox} is far more sensitive to bgNO_x than to NO_xemis. As BLH may only affect f_{ox} in the P6 parameterization through the dilution of NO_x emissions, f_{ox} is also insensitive to BLH. The value of f_{ox} is determined by the remaining four inputs. The value of f_{ox} increases with increasing time since emission, and so nearly linearly increases with increasing d and is nearly inversely proportional to v_g. The dependance of f_{ox} on DSWRF and

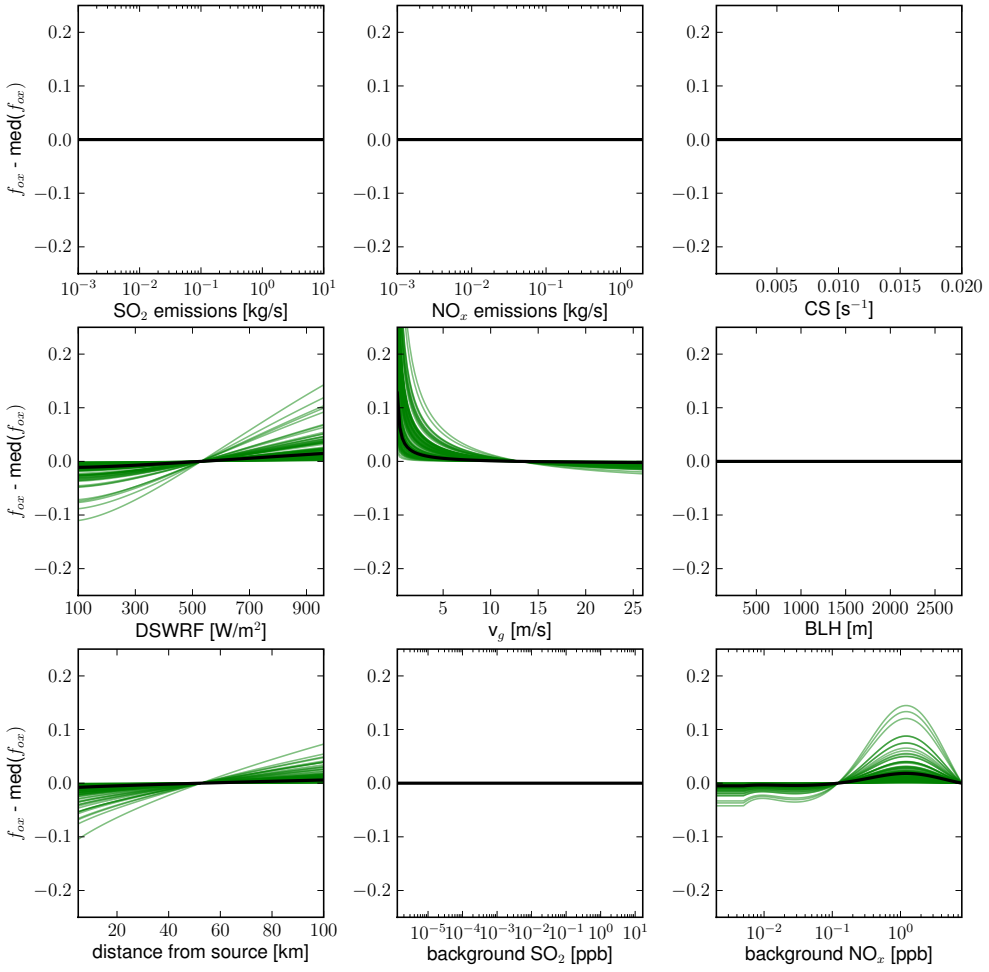

Fig. 2. Sensitivity of f_{ox} to each of the inputs for 100 randomly selected sample inputs. The black line denotes the median value case. The median value of each plotted line is subtracted from its values to highlight the sensitivities to the inputs.

bgNO_x is determined largely by the dependance of OH on these two variables, as parameterized in SAM-TOMAS. The value increases with increasing DSWRF, and there is a peak in f_{ox} at bgNO_x equal to 1 ppb.

The value of M_m is much more sensitive to NO_xemis than to bgNO_x, unlike f_{ox}. Concentrations of SO_2 are highest close to the source, so concentrations of H_2SO_4 (and particle growth rates) may also be highest close to the source, even if SO_2 is being oxidized more slowly. The concentrations of H_2SO_4 close to the source will be more sensitive to NO_x emissions than to background NO_x concentrations, and therefore M_m is also more sensitive to NO_xemis than bgNO_x. This is also reflected in the dependencies of M_m on d and on v_g. The value of f_{ox} is nearly linearly increasing with d, while M_m increases at low values of d but becomes insensitive at higher values. The value of M_m is much less sensitive than f_{ox} to v_g, although this is convoluted by the effect of v_g on M_m through dilution of SO_2 and NO_x emissions, which is also the cause of the slight dependance of M_m on BLH. There is a decrease in M_m with increasing CS due to the loss in available H_2SO_4 to pre-existing particles. We also note that M_m becomes insensitive to SO_2emis, bgSO_2, and bgNO_x, as well as NO_xemis under some conditions, at small values of each of these inputs. If the background concentrations of NO_x or SO_2 are sufficiently low compared to emissions, in-plume NO_x or SO_2 will be dominated by the emissions, and so further reductions in the background concentrations will not significantly affect M_m. The reverse is also true if the emissions are sufficiently low compared to the background concentrations.

The value of N_{new} depends on the inputs in a similar manner to M_m. It decreases with increasing CS due to both removal of new particles by coagulation and competition for available H_2SO_4. It increases with increasing DSWRF. The value of N_{new} is more sensitive to NO_xemis than to bgNO_x. However, N_{new} increases with increasing bgSO_2 but decreases with increasing SO_2emis. Increases in either emissions of SO_2 or the background concentration of SO_2 will

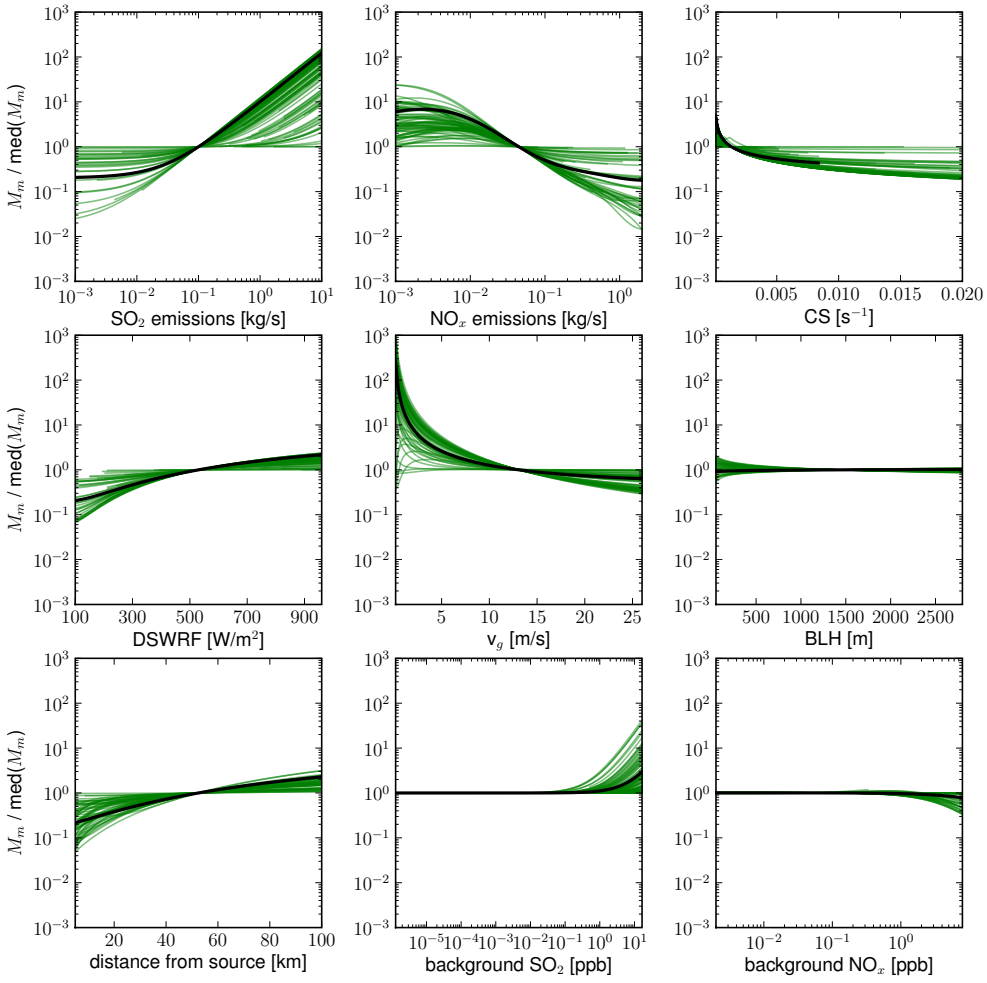

Fig. 3. Sensitivity of M_m to each of the inputs for 100 randomly selected sample inputs. If nucleation is not predicted by the P6 parameterization, no value is shown. The black line denotes the median value case. Each plotted line is divided by its median value in order to highlight the sensitivities to the inputs.

increase the available H_2SO_4, thus increasing new-particle formation, but because N_new is defined as the number of new particles normalized by the emissions of SO_2, and emissions of SO_2 less than linearly increase the number of new particles, increases in the emissions of SO_2 have a small decreasing effect on N_new. The value of N_new also has a complex dependance on v_g and d, either increasing or decreasing with increasing d and decreasing v_g. As the time since emission (d/v_g) increases, N_new will increase due to continuing new-particle formation and will decrease due to coagulational scavenging by pre-existing particles. The dependance of N_new on d and v_g will depend on the competition between these two processes. We do note, however, that N_new tends to asymptote to a single value with increasing d, depending on the values of the other inputs.

Of the four outputs of the P6 parameterization, f_new shows the most dramatic changes for small changes in some of the inputs. Specifically, f_new is sensitive to small changes for high values of SO_2emis, high values of bgSO_2, low values of CS, and, for some combinations of inputs, low values of v_g. The value of f_new is less sensitive to the remaining variables, but increases for increasing DSWRF and d, decreases slightly for increasing BLH, and generally decreases with decreasing bgNO_x.

5.2 Sensitivity to number of sources assumed

Often, anthropogenic emissions inventories give emissions of SO_2 and NO_x on a given grid, and not per point source. Figure 6 shows the sensitivity of the P6 parameterization to assumptions about how these emissions are split between sources within the grid box. We used the P6 parameterization to predict f_ox, M_m, N_new, and f_new for 100 different sets of inputs randomly chosen from the range of values tested for each variable, assuming the emissions were split evenly amongst between 1 and 10 point sources. We also show the

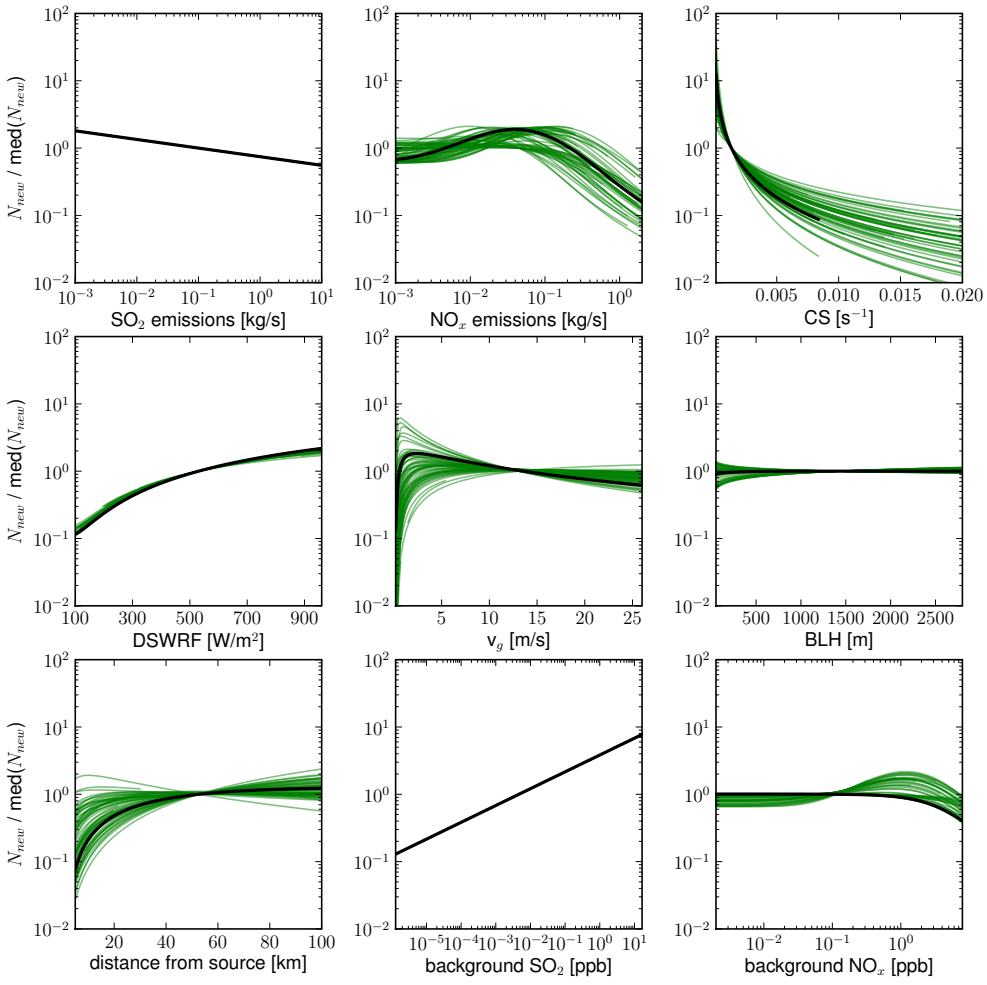

Fig. 4. Sensitivity of N_{new} to each of the inputs for 100 randomly selected sample inputs. If nucleation is not predicted by the P6 parameterization, no value is shown. The black line denotes the median value case. Each plotted line is divided by its median value in order to highlight the sensitivities to the inputs.

sensitivity for the median case, as we did in Figs. 2, 3, 4, and 5. As in Figs. 2, 3, 4, and 5, we shift the lines vertically to highlight the sensitivities by subtracting the median value of each plotted line from its values for f_{ox} and f_{new} and dividing each plotted line by its median value for M_{m} and N_{new}. We do not show values for M_{m}, N_{new}, and f_{new} for cases where no nucleation is predicted. As the value of f_{ox} is insensitive to both SO_2emis and NO_xemis, it is also completely insensitive to assumptions about the number of point sources. Since M_{m} increases with increasing SO_2emis but decreases with increasing NO_xemis across most of the ranges of these two variables, M_{m} may increase or decrease as the emissions are split amongst additional sources. The value of N_{new} decreases with increasing SO_2emis but peaks for NO_xemis values near 0.05 kg s^{-1}, and so may also increase or decrease as NO_xemis is split amongst a larger number of sources. We tested 10 000 randomly generated samples within the range of inputs used for the training data, and for an increase in the number of sources from 1 to 10, the values of M_{m} and N_{new} stayed within a factor of 3 for 64 and 85 % of the cases, respectively (note that values for M_{m} and N_{new} span 5 and 3 orders of magnitude, so a factor of 3 change is small compared to this range). The value for f_{new} can change more dramatically for large values of SO_2emis, but the change was less than ± 0.01 for 78 % of the samples tested.

As discussed earlier, we include three different options for specifying SO_2 and NO_x emissions in our included Fortran code of the P6 parameterization. Two of these options involve specifying the total emissions in the grid box and allowing P6 to make assumptions about the size of the sources (Table 3). Fortunately, the analysis above shows that the P6 outputs are generally not very sensitive to the number of sources assumed, so the lack of knowledge of individual sources likely will not create large errors in P6 outputs.

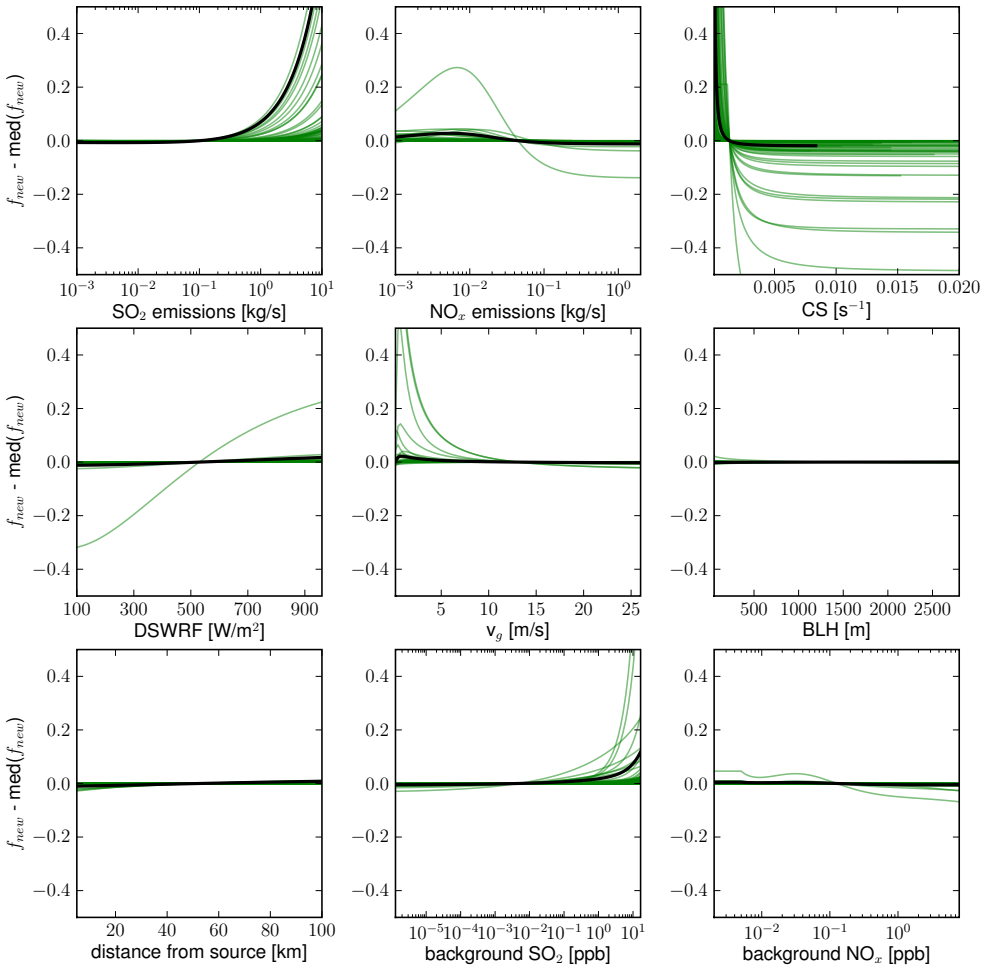

Fig. 5. Sensitivity of f_{new} to each of the inputs for 100 randomly selected sample inputs. If nucleation is not predicted by the P6 parameterization, no value is shown. The black line denotes the median value case. The median value of each plotted line is subtracted from its values to highlight the sensitivities to the inputs.

6 Conclusions

In this study, we describe the predicting particles produced in power-plant plumes (P6) parameterization: a physically based, but computationally efficient, parameterization that predicts the characteristics of aerosol formed in sulfur-rich plumes based on variables that are commonly available in global- and regional-scale models. The parameterization predicts the fraction of the emitted SO_2 that is oxidized to form H_2SO_4, the fraction of that H_2SO_4 that forms new particles, the mean mass per particle of the new particles, and the number of new particles per kg SO_2 emitted. It takes as inputs the source-level SO_2 and NO_x emissions rates, the background aerosol condensation sink, the downward shortwave radiative flux, the mean boundary-layer wind speed, the boundary-layer height, the background SO_2 and NO_x concentrations, and the distance from the source. The increase in running time of a 3-D aerosol model due to implementing the P6 parameterization would be negligible because the parameterization consists only of several arithmetic equations.

In order to create a set of training data for the P6 parameterization, we used the SAM-TOMAS LES/CRM model with online aerosol microphysics. We have shown that the results of the parameterization show good agreement with the results of the SAM-TOMAS model and that the P6 parameterization captures the variability in aerosol formation and growth in sulfur-rich plumes, with correlation coefficients ranging from 0.650 for f_{new} to 0.891 for f_{ox}.

While the P6 parameterization reproduces well the behaviour of the SAM-TOMAS model, we note that it inherits the limitations of the SAM-TOMAS model. Aqueous-phase oxidation of SO_2 is not accounted for, and therefore f_{ox} may be underpredicted under cloudy conditions. Nitrous acid (HONO) and sulfur trioxide (SO_3) emission are not accounted for, and these processes may result in particle formation early in the plume. Nucleation rates are parameterized using an empirical fit proportional to H_2SO_4 concentrations.

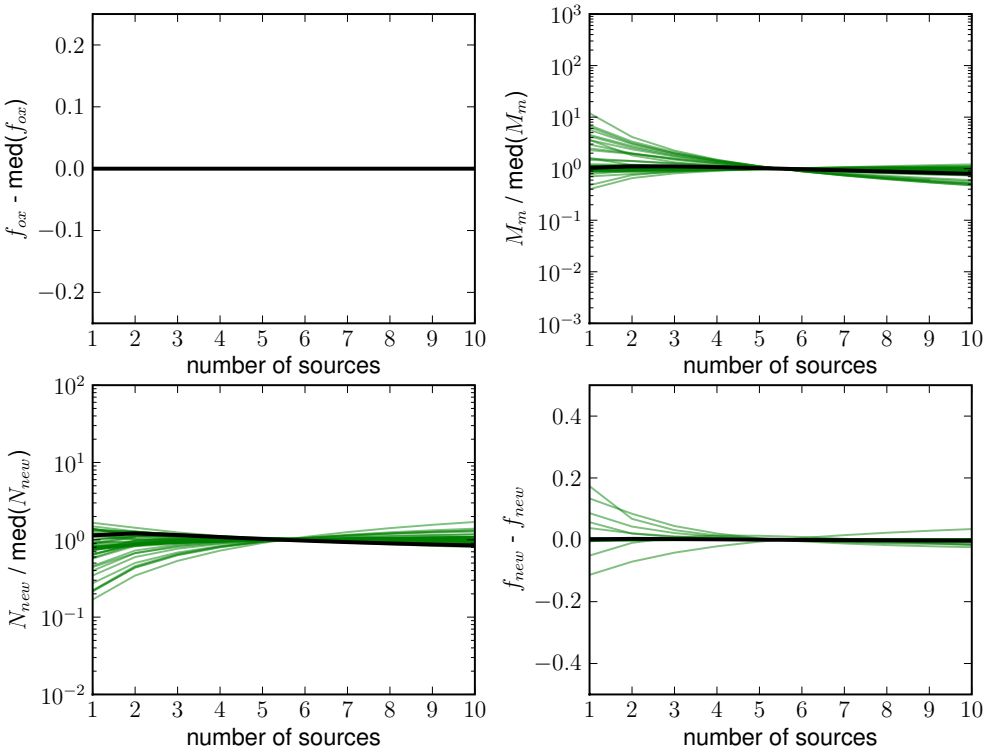

Fig. 6. Sensitivity of f_{ox}, M_{m}, N_{new}, and f_{new} to the assumed number of emission sources, while keeping total emissions of SO_2 and NO_x constant, for 100 randomly selected sets of inputs. If nucleation is not predicted by the P6 parameterization, no value is shown. The black line in each figure denotes the median value case. In order to highlight the sensitivities to the number of sources assumed, for f_{ox} and f_{new}, the median value of each plotted line is subtracted from the line, and for M_{m} and N_{new}, each plotted line is divided by its median value.

Despite these limitations, the SAM-TOMAS model has been previously shown to well represent the formation and growth of aerosol in coal-fired power-plant plumes (Stevens et al., 2012; Lonsdale et al., 2012). We therefore believe that the P6 parameterization captures well the variability in new-particle formation and growth within sulfur-rich plumes.

The median value of f_{ox} predicted by the P6 parameterization (0.0098) for the training cases is much less than the fraction of emitted SO_2 mass added as sub-grid sulfate by Adams and Seinfeld (2003) (0.03) or Dentener et al. (2006) (0.025). Additionally, we excluded night-time cases from our training data, where no oxidation of SO_2 and no new-particle formation would be predicted by the P6 parameterization. Consequently, we expect that predictions of total aerosol mass near sulfur-rich point sources using global-scale models implementing the P6 parameterization will be less than those using the Adams and Seinfeld (2003) or Dentener et al. (2006) assumptions. Additionally, as the median values of both N_{new} and M_{m} predicted by SAM-TOMAS were less than those predicted by Adams and Seinfeld (2003), we expect than both globally averaged aerosol number concentrations and globally averaged CCN concentrations would be less than those using the Adams and Seinfeld (2003) assumption, with large regional differences (e.g. less CCN formation using the P6 parameterization under cloudy, polluted conditions than sunny, low-background-aerosol conditions). It is our intent to perform a complete comparison of the results of a global chemical-transport model with and without the parameterization as a future work.

This parameterization will allow for improved representation of sub-grid formation and growth of sulfate aerosol in global- and regional-scale models, allowing for more accurate predictions of aerosol size distributions and improved confidence in studies of aerosol effects on health and climate.

Appendix A

What if one or more of the P6 inputs are not available?

SO_2emis, NO_xemis: if no estimate of the SO_2 emissions is available, the P6 parameterization can be run assuming a representative distribution of power plants within the area. This is described in more detail in Sect. 3. If the total NO_x emissions are unknown, the parameterization will assume a SO_2emis : NO_xemis ratio of 0.419 based on the 2010 CAM data.

DSWRF: the clear-sky. DSWRF can be calculated by

$$\mathrm{dswrf} = S_0 T \cos(\mathrm{sza}),$$

where S_0 is the solar constant at the top of the atmosphere, 1370 W m^{-2}, T is the transmittance of the atmosphere, and sza is the solar zenith angle. The clear-sky transmittance has a value of about 0.76 (globally averaged; Seinfeld and Pandis, 2006), and the solar zenith angle can be calculated based on the latitude, longitude, time of day, and day of year. This approximation will typically overestimate DSWRF as it assumes no cloud cover. If no input is given, a value of 400 W m^{-2} will be assumed.

CS: the value of CS can be approximated based on a typical aerosol background for the location in question. We note that the typical aerosol size distributions listed in Seinfeld and Pandis (2006) for urban, rural, remote continental, and marine conditions correspond to condensation sinks of 0.060, 0.0063, 0.011, and 0.0010 s^{-1}, respectively. Also, the remote continental size distribution yields a PM_{10} mass concentration of 25.88 µg m^{-3}, so we suggest that CS may be estimated from PM_{10} mass concentrations by multiplying by 4.3×10^{-4} s^{-1}/(µg m^{-3}). If no input is given, we will assume the value for a remote continental case, 0.011 s^{-1}.

v_g: the value of v_g must be assumed if not known. We choose a typical value of 6 m s^{-1} if no input is given.

BLH: the BLH can be approximated by typical values for the location and time of day. If no value is given, a value of 500 m will be assumed.

d: we recognize that there is some ambiguity about what value should be used as input for d by global- and regional-scale model users. One interpretation is that d is the distance where the air mass passing over the source enters the next adjacent grid cell. Another is the distance where the width of the plume equals the grid width, allowing the plume to be resolved. However, solving for either of these distances under changing wind direction and meteorological conditions is not a trivial task even if the location of the power plant within the grid cell is known, and often the location will not be available. We suggest then that users of our parameterization use half the horizontal grid cell resolution as an approximation for d. We show in our sensitivity studies that for distances greater than 30 km, M_m, N_{new}, and f_{new} are not strongly dependant on d, and f_{ox} is a less-than-linear function of d.

bgSO_2, bgNO_x: following Table 2.7 of Seinfeld and Pandis (2006), we suggest values of bgNO_x of 10 ppb for urban locations, 1 ppb for rural locations, and 0.05 ppb for remote locations. For bgSO_2 we suggest values of 10 ppb for urban locations, 0.5 ppb for remote continental conditions, and 0.05 ppb for marine conditions. If no input is given, values of 0.5 and 1 ppb are used for bgSO_2 and bgNO_x.

Appendix B

Summary of equations necessary for each output

We note that the full parameterization is available programmed in Fortran 90 as a supplement. However, if the provided code is insufficient for the users' needs, we request that the users contact the authors to find out if the P6 parameterization has already been translated into the necessary programming language, if the necessary adjustments have already been made, or if an updated version is available. In the case where this still proves insufficient, we summarize in this appendix which equations from the preceding manuscript are necessary to calculate each output. We strongly recommend that users consult the preceding manuscript for a full discussion of caveats and assumptions associated with the P6 parameterization. We also recommend that users ensure that they use the correct value from Table 5 whenever they use Eq. (1) or Eq. (9).

Fraction of SO_2 oxidized (f_{ox}):

Equations 1–6, 8 (2nd row from Table 5).

Nucleation:

Equations 1, 9, 10 (3rd row from Table 5).

Mean mass of new particles (M_m):

First, determine if significant nucleation has occurred (M_m is poorly defined otherwise):

Equations 1, 9, 10 (3rd row from Table 5).

Then calculate $f_{ox,eff}$: Eqs. 1–6, 8 (4th row from Table 5).

Then Eq. 11.

If also using f_{new}, calculate it now as noted below. If $f_{new} > 1$, divide M_m by $f_{new}^{0.5}$ to maintain closure.

Median diameter of new particles (D_m):

Calculate M_m as noted above. Then Eqs. 12, 13.

Number of new particles per kg SO_2 (N_{new}):

First, determine if significant nucleation has occurred (N_{new} very small otherwise):

Equations (1), (9), (10) (3rd row from Table 5).

Then calculate $f_{ox,eff}$: Eqs. (1)–(6), (8) (4th row from Table 5).

Then Eq. (11).

If also using f_{new}, calculate it now as noted below. If $f_{new} > 1$, divide N_{new} by $f_{new}^{0.5}$ to maintain closure.

Fraction of sulfate mass that comprises new particles (f_{new}):

Calculate f_{ox}, M_m, and N_{new} as noted above. Then use Eq. 15.

Supplementary material related to this article is available online at http://www.atmos-chem-phys.net/13/12117/2013/acp-13-12117-2013-supplement.zip.

Acknowledgements. We thank the Atlantic Computational Excellence Network (ACENet) for the computational resources used in this study. We also thank the Natural Sciences and Engineering Research Council (NSERC) of Canada for funding.

Edited by: D. Topping

References

Adams, P. J. and Seinfeld, J. H.: Predicting global aerosol size distributions in general circulation models, J. Geophys. Res., 107, 1–23, doi:10.1029/2001JD001010, 2002.

Adams, P. J. and Seinfeld, J. H.: Disproportionate impact of particulate emissions on global cloud condensation nuclei concentrations, Geophys. Res. Lett., 30, 1239, doi:10.1029/2002GL016303, 2003.

Albrecht, B.: Aerosols, cloud microphysics, and fractional cloudiness., Science, New York, NY, 245, 1227–1230, 1989.

Bey, I., Jacob, D. J., Yantosca, R. M., Logan, J. a., Field, B. D., Fiore, A. M., Li, Q., Liu, H. Y., Mickley, L. J., and Schultz, M. G.: Global modeling of tropospheric chemistry with assimilated meteorology: Model description and evaluation, J. Geophys. Res., 106, 23073, doi:10.1029/2001JD000807, 2001.

Charlson, R. J., Schwartz, S. E., Hales, J. M., Cess, R. D., Coakley, J. a, Hansen, J. E., and Hofmann, D. J.: Climate forcing by anthropogenic aerosols, Science, New York, NY, 255, 423–430, doi:10.1126/science.255.5043.423, 1992.

Dentener, F., Kinne, S., Bond, T., Boucher, O., Cofala, J., Generoso, S., Ginoux, P., Gong, S., Hoelzemann, J. J., Ito, A., Marelli, L., Penner, J. E., Putaud, J. P., Textor, C., Schulz, M., Van Der Werf, G. R., and Wilson, J.: Emissions of primary aerosol and precursor gases in the years 2000 and 1750 prescribed data-sets for AeroCom, Atmos. Chem. Phys., 6, 4321–4344, doi:10.5194/acp-6-4321-2006, 2006.

Dockery, D., Pope, C., Xu, X., Spengler, J. D., Ware, J. H., Fay, M. E., Ferris, B. G., and Speizer, F. E.: An association between air pollution and mortality in six US cities, New England Journal of Medicine, 329(24), 1753–1759, doi:10.1056/NEJM199312093292401, 1993.

Dusek, U., Frank, G. P., Hildebrandt, L., Curtius, J., Schneider, J., Walter, S., Chand, D., Drewnick, F., Hings, S., Jung, D., Borrmann, S., and Andreae, M. O.: Size matters more than chemistry for cloud-nucleating ability of aerosol particles, Science New York, NY, 312, 1375–1378, doi:10.1126/science.1125261, 2006.

Forster, P., Ramaswamy, V., Artaxo, P., Berntsen, T., Betts, R., Fahey, D. W., Haywood, J., Lean, J., Lowe, D. C., Myhre, G., Nganga, J., Prinn, R., Raga, G., Schulz, M., and Dorland, R. V.: Changes in Atmospheric Constituents and in Radiative Forcing, in Climate Change 2007: The Physical Science Basis, Contribution of Working Group I to the Fourth Assessment Report of the Intergovernmental Panel on Climate Change, edited by: Miller, H. L., 129–234, Cambridge University Press, Cambridge, UK and New York, NY, USA, 2007.

Kerminen, V., Lehtinen, K., Anttila, T., and Kulmala, M.: Dynamics of atmospheric nucleation mode particles: a timescale analysis, Tellus B, 56, 135–146, 2004.

Khairoutdinov, M. and Randall, D.: Cloud resolving modeling of the ARM summer 1997 IOP: Model formulation, results, uncertainties, and sensitivities, Journal of the Atmospheric Sciences, 60, 607–626, doi:10.1175/1520-0469(2003)060<0607:CRMOTA>2.0.CO;2, 2003.

Kulmala, M. and Kerminen, V.-M.: On the formation and growth of atmospheric nanoparticles, Atmos. Res., 90, 132–150, doi:10.1016/j.atmosres.2008.01.005, 2008.

Kulmala, M., Lehtinen, K. and Laaksonen, A.: Cluster activation theory as an explanation of the linear dependence between formation rate of 3 nm particles and sulphuric acid concentration, Atmos. Chem. Phys., 6, 787–793, doi:10.5194/acpd-6-787-2006, 2006.

Lee, L. A., Pringle, K. J., Reddington, C. L., Mann, G. W., Stier, P., Spracklen, D. V., Pierce, J. R., and Carslaw, K. S.: The magnitude and causes of uncertainty in global model simulations of cloud condensation nuclei, Atmos. Chem. Phys., 13, 8879–8914, doi:10.5194/acp-13-8879-2013, 2013.

Lonsdale, C. R., Stevens, R. G., Brock, C. A., Makar, P. A., Knipping, E. M., and Pierce, J. R.: The effect of coal-fired power-plant SO_2 and NO_x control technologies on aerosol nucleation in the source plumes, Atmos. Chem. Phys., 12, 11519–11531, doi:10.5194/acp-12-11519-2012, 2012.

Luo, G. and Yu, F.: Sensitivity of global cloud condensation nuclei concentrations to primary sulfate emission parameterizations, Atmos. Chem. Phys., 11, 1949–1959, doi:10.5194/acp-11-1949-2011, 2011.

Makkonen, R., Asmi, a., Korhonen, H., Kokkola, H., Järvenoja, S., Räisänen, P., Lehtinen, K. E. J., Laaksonen, a., Kerminen, V.-M., Järvinen, H., Lohmann, U., Bennartz, R., Feichter, J., and Kulmala, M.: Sensitivity of aerosol concentrations and cloud properties to nucleation and secondary organic distribution in ECHAM5-HAM global circulation model, Atmos. Chem. Phys., 9, 1747–1766, doi:10.5194/acp-9-1747-2009, 2009.

Mauldin, R. L., Berndt, T., Sipilä, M., Paasonen, P., Petäjä, T., Kim, S., Kurtén, T., Stratmann, F., Kerminen, V.-M., and Kulmala, M.: A new atmospherically relevant oxidant of sulphur dioxide., Nature, 488, 193–196, doi:10.1038/nature11278, 2012.

Mesinger, F., DiMego, G., Kalnay, E., Mitchell, K., Shafran, P. C., Ebisuzaki, W., Jovic', D., Woollen, J., Rogers, E., Berbery, E. H., Ek, M. B., Fan, Y., Grumbine, R., Higgins, W., Li, H., Lin, Y., Manikin, G., Parrish, D., and Shi, W.: North American Regional Reanalysis, B. Am. Meteor. Soc., 87, 343–360, doi:10.1175/BAMS-87-3-343, 2006.

Olson, J. R., Crawford, J. H., Chen, G., Brune, W. H., Faloona, I. C., Tan, D., Harder, H., and Martinez, M.: A reevaluation of airborne HO x observations from NASA field campaigns, J. Geophys. Res., 111, D10301, doi:10.1029/2005JD006617, 2006.

Peters, A., Wichmann, H. E., Tuch, T., Heinrich, J. and Heyder, J.: Respiratory effects are associated with the number of ultrafine particles, Am. J. Resp. Crit. Care Med., 155, 1376–1383, 1997.

Pierce, J. R. and Adams, P. J.: Global evaluation of CCN formation by direct emission of sea salt and growth of ultrafine sea salt, J. Geophys. Res., 111, D06203, doi:10.1029/2005JD006186, 2006.

Pierce, J. R. and Adams, P. J.: Uncertainty in global CCN concentrations from uncertain aerosol nucleation and primary emission

rates, Atmos. Chem. Phys., 9, 1339–1356, doi:10.5194/acp-9-1339-2009, 2009.

Pierce, J. R., Chen, K. and Adams, P. J.: Contribution of primary carbonaceous aerosol to cloud condensation nuclei: processes and uncertainties evaluated with a global aerosol microphysics model, Atmos. Chem. Phys., 7(20), 5447–5466, doi:10.5194/acp-7-5447-2007, 2007.

Pierce, J. R., Evans, M. J., Scott, C. E., D'Andrea, S. D., Farmer, D. K., Swietlicki, E., and Spracklen, D. V.: Weak global sensitivity of cloud condensation nuclei and the aerosol indirect effect to Criegee + SO_2 chemistry, Atmos. Chem. Phys., 13, 3163–3176, doi:10.5194/acp-13-3163-2013, 2013.

Seinfeld, J. H. and Pandis, S. N.: Atmos. Chem. Phys.: From Air Pollution to Climate Change, 2nd ed., John Wiley and Sons, Inc., Hoboken, New Jersey, p. 371 and p. 1069, 2006.

Snow-Kropla, E. J., Pierce, J. R., Westervelt, D. M., and Trivitayanurak, W.: Cosmic rays, aerosol formation and cloud-condensation nuclei: sensitivities to model uncertainties, Atmos. Chem. Phys., 11, 4001–4013, doi:10.5194/acp-11-4001-2011, 2011.

Spracklen, D. V., Pringle, K. J., Carslaw, K. S., Chipperfield, M. P., and Mann, G. W.: A global off-line model of size-resolved aerosol microphysics: I. Model development and prediction of aerosol properties, Atmos. Chem. Phys., 5, 2227–2252, doi:10.5194/acp-5-2227-2005, 2005.

Stevens, R. G., Pierce, J. R., Brock, C. A., Reed, M. K., Crawford, J. H., Holloway, J. S., Ryerson, T. B., Huey, L. G., and Nowak, J. B.: Nucleation and growth of sulfate aerosol in coal-fired power plant plumes: sensitivity to background aerosol and meteorology, Atmos. Chem. Phys., 12, 189–206, doi:10.5194/acp-12-189-2012, 2012.

Trivitayanurak, W., Adams, P. J., Spracklen, D. V., and Carslaw, K. S.: Tropospheric aerosol microphysics simulation with assimilated meteorology: model description and intermodel comparison, Atmos. Chem. Phys., 8, 3149–3168, doi:10.5194/acp-8-3149-2008, 2008.

Twomey, S.: Pollution and planetary albedo, Atmos. Environ., 8, 1251–1256, doi:10.1016/0004-6981(74)90004-3, 1974.

United States Environmental Protection Agency: Clean Air Markets: Data and Maps, available at: http://ampd.epa.gov/ampd/ (last access: March 2013), 2012.

Wang, M. and Penner, J. E.: Aerosol indirect forcing in a global model with particle nucleation, Atmos. Chem. Phys., 9, 239–260, doi:10.5194/acp-9-239-2009, 2009.

Yu, F.: Diurnal and seasonal variations of ultrafine particle formation in anthropogenic SO2 plumes., Environ. Sci. Technol., 44, 2011–2015, doi:10.1021/es903228a, 2010.

Yu, F. and Luo, G.: Simulation of particle size distribution with a global aerosol model: contribution of nucleation to aerosol and CCN number concentrations, Atmos. Chem. Phys., 9, 7691–7710, doi:10.5194/acp-9-7691-2009, 2009.

Zhou, W., Cohan, D. S., Pinder, R. W., Neuman, J. A., Holloway, J. S., Peischl, J., Ryerson, T. B., Nowak, J. B., Flocke, F., and Zheng, W. G.: Observation and modeling of the evolution of Texas power plant plumes, Atmos. Chem. Phys., 12, 455–468, doi:10.5194/acp-12-455-2012, 2012.